Variability of the Solar Wind Flow Asymmetry in the Martian Magnetosheath observed by MAVEN

N. Romanelli[1,2], G. DiBraccio[1], J. Halekas[3], E. Dubinin[4], J. Gruesbeck[1], J. Espley[1], G. Poh[1,5], Y. Ma[6], and J. G. Luhmann[7]

[1]Planetary Magnetospheric Laboratory, NASA Goddard Space Flight Center, USA.
[2]CRESST II,University of Maryland, Baltimore County, USA.
[3]Department of Physics and Astronomy, University of Iowa, Iowa City, IA, USA.
[4]Max-Planck-Institute for Solar System Research, Göttingen, Germany.
[5]CRESST II, Catholic University of America, Washington DC, USA.
[6]Department of Earth, Planetary, and Space Sciences, University of California, Los Angeles, CA, USA.
[7]Space Sciences Laboratory, University of California, Berkeley, CA, USA.

Key Points:

- The solar wind is deflected asymmetrically around Mars as a result of massloading by oxygen ions derived from the extended oxygen corona.
- MAVEN data reveal a linear correlation between the flow asymmetry and the IMF cross-flow component to the solar wind proton density ratio.
- The asymmetry can be understood by means of a two-fluid description, with boundary conditions defined by the pristine solar wind properties.

Corresponding author: Norberto Romanelli, `norberto.romanelli@nasa.gov`, `https://orcid.org/0000-0001-9210-0284`

Abstract

We perform the first statistical analysis of effects that different external conditions have on a solar wind (SW) flow asymmetry observed in the Martian magnetosheath due to mass loading, making use of $\sim$ 5 years of Mars Atmosphere and Volatile EvolutioN (MAVEN) observations. We find the difference between the mean magnetosheath SW velocity component along the SW convective electric field direction in regions in the positive and negative hemispheres displays a strong linear correlation with the ratio between the upstream Interplanetary Magnetic Field (IMF) cross-flow component (B_y) and the SW proton density (n_{sw}). The asymmetry is maximized ($\sim$ 25 - 35 km s^{-1}) for low n_{sw} ($\sim$ 1 cm^{-3}) and large IMF B_y ($\sim$ 2 nT). These results suggest the SW flow asymmetry variability is due to a force arising from the differential streaming between SW protons and oxygen ions, with boundary conditions partly defined by the pristine SW properties.

Plain Language Summary

In this work we study a solar wind flow asymmetry observed in the Martian magnetosheath that is an indirect result of the presence of an extended oxygen corona. This asymmetry is due to the lateral deflection of the oxygen ion-massloaded solar wind in the direction opposite to that of the solar wind convective electric field. In turn, this deflection can be understood in terms of total linear momentum conservation, since oxygen ions are initially accelerated along the latter field. By analyzing Mars Atmosphere and Volatile EvolutioN magnetic field and plasma observations we find that this asymmetry is observed more clearly for relatively low solar wind proton density and large Interplanetary Magnetic Field cross-flow component values. The results emphasize the influence of pristine solar wind properties in the shocked solar wind deflection around Mars and its interaction with the oxygen corona.

1 Introduction

The lack of a global dynamo-generated magnetic field at Mars results in the direct interaction between the solar wind (SW) and the Martian atmosphere, ionosphere and crustal magnetic fields (Acuña et al., 1998). This interaction starts upstream from the Martian bow shock, due to the presence of the extended hydrogen exosphere and oxygen corona (e.g., Chaffin et al., 2014, 2015; Chaufray et al., 2008; Clarke et al., 2017; Deighan et al., 2015; Feldman et al., 2011; Halekas, 2017). In particular, newborn planetary protons (H^+) and oxygen ions (O^+) are picked-up at these locations and in the Martian magnetosheath by the magnetized SW, as reported by Barabash et al. (1991); Curry et al. (2015); Dubinin et al. (2006); Rahmati et al. (2015, 2017); Yamauchi et al. (2015); Dong et al. (2015). In addition to contributing to planetary escape, such picked-up ions are responsible, among other outcomes, for the presence of different plasma instabilities (e.g., Russell et al., 1990; Brain et al., 2002; Bertucci et al., 2013; Mazelle et al., 2004; Romanelli et al., 2013, 2016; Ruhunusiri et al., 2015, 2016; Liu et al., 2020; Halekas et al., 2020; Andrés et al., 2020).

Oxygen planetary ions created in the SW and the magnetosheath initially follow cycloidal trajectories in the SW velocity ($\mathbf{V}_{sw}$) - SW convective electric field ($\mathbf{E}_{SW}$) plane. Given that the upstream O^+ pick-up gyroradius ($\sim 5\ R_M$ for $|B| \sim 4$ nT, where R_M stands for Mars's radii) exceeds the characteristic size of the Martian magnetosphere, deflected O^+ ions initially gain linear momentum transverse to the Mars-Sun line and along the SW convective electric field direction. If the solar wind-oxygen ions electromagnetic interaction can be considered an isolated system, this momentum gain must be balanced by a deflection of the SW protons in the direction opposite to that of $\mathbf{E}_{SW}$. Signatures associated with such SW deflection have been observed both upstream from the Martian bow shock (Halekas, Ruhunusiri, et al., 2017) and in the Martian magnetosheath (Dubinin et al., 2018). Analogous but more pronounced SW deflection has also been recently observed around comet 67P/Churyumov-Gerasimenko (e.g., Broiles et al., 2015; Nilsson et al., 2015, 2017; Behar et al., 2016, 2017; Glassmeier, 2017). In particular, Dubinin et al. (2018) studied the associated asymmetry in the SW flow deflection in the Martian magnetosheath by analyzing Mars Atmosphere and Volatile EvolutioN (MAVEN) Solar Wind Ion Analyzer (SWIA) and Suprathermal and Thermal Ion Composition (STATIC) observations, obtained between November 2014 and May 2016 (McFadden et al., 2015; Halekas et al., 2015; Jakosky et al., 2015). The authors concluded that the observed asymmetry can be attributed to the previously mentioned effects of oxygen ions mass-loading the SW. It is important to point out that, in principle, an analogous solar wind response should take place as a result of the planetary pick up protons (Barabash et al., 1991; Dubinin et al., 2006; Rahmati et al., 2017). However, given their relatively low mass and number densities, the SW linear momentum is slightly affected by their presence (Dubinin et al., 2018).

The macroscopic forces acting on the SW protons and oxygen planetary ions can be approximated by means of a two-fluid description, taking into account the momentum exchange between them and finite Larmor effects present in the Martian magnetosheath (Sauer et al., 1994; Halekas, Brain, et al., 2017; Dubinin et al., 2018). In this description, the momentum equations for the SW protons and planetary O^+ ions are:

$$m_p n_p \frac{d\mathbf{V}_p}{dt} = \frac{n_p}{n_e}\left[\mathbf{J}\times\mathbf{B} - \nabla p_e + e n_{o^+}(\mathbf{V}_p - \mathbf{V}_{o^+})\times\mathbf{B}\right] - \nabla\cdot\mathbf{P}_p \tag{1}$$

$$m_{o^+} n_{o^+} \frac{d\mathbf{V}_{o^+}}{dt} = \frac{n_{o^+}}{n_e}\left[\mathbf{J}\times\mathbf{B} - \nabla p_e + e n_p(\mathbf{V}_{o^+} - \mathbf{V}_p)\times\mathbf{B}\right] - \nabla\cdot\mathbf{P}_{o^+} \tag{2}$$

where, m_p,$\mathbf{V}_p$, n_p, m_{o^+} $\mathbf{V}_{o^+}$, n_{o^+} are the mass, velocity and number density of protons and oxygen ions, respectively. $\mathbf{J}$ and $\mathbf{B}$ are the current density and the magnetic field, respectively, and n_e, ∇p_e and $\nabla\cdot\mathbf{P}_i$ are electron number density, the scalar electron pressure and the tensor ion pressure.

Compared to the single fluid MHD approximation, an additional term is therefore associated with the differential streaming of the proton and oxygen ion fluids. As shown by Halekas, Brain, et al. (2017), the $\mathbf{V}_p\times\mathbf{B}$ field greatly exceeds the thermal and magnetic pressure gradient terms in strength, in the upstream, magnetosheath, and flank regions. In particular, this field has the strongest component along the $\mathbf{E}_{SW}$ direction in the $\mathbf{V}_{sw}-\mathbf{E}_{SW}$ plane, also inside the Martian magnetosheath. In addition, given that $\mathbf{V}_{o^+}$ points mainly along $\mathbf{E}_{SW}$ (at least for a newborn heavy ion) the $\mathbf{V}_{o^+}\times\mathbf{B}$ term points mainly along the Mars-Sun direction. Therefore, under these conditions, one could expect that the force associated with the differential streaming between the ion fluids can be the leading term along the $\mathbf{E}_{SW}$ direction in the magnetosheath, for a given n_{o^+} density range. Under these conditions Equation (1) is reduced to:

$$\frac{d\mathbf{V}_p}{dt} = -\frac{e\, n_{o^+}}{m_p\, n_e}\mathbf{E}_{SW} \tag{3}$$

where $\mathbf{E}_{SW} = -\mathbf{V}_p \times \mathbf{B}$. Equation (3) explicitly shows that under these conditions, approximately valid upstream from the Martian bow shock, the SW protons should be deflected opposite to $\mathbf{E}_{SW}$. As a consequence, the presence of this preferential direction partly breaks the expected symmetry of the SW deflection around Mars downstream from the bow shock.

Moreover, given that the solution to Equation (1) requires an integration along the SW streamlines that takes into account the boundary conditions (partly given by Equation 3), these theoretical considerations suggest a dependence of the SW flow deflection asymmetry in the Martian magnetosheath on the SW external conditions, in particular, on $|\mathbf{E}_{SW}|/n_e$.

Additional MAVEN magnetic field and plasma data are currently available to build upon the original work by Dubinin et al. (2018) to investigate the cause and variability of this asymmetry. In this work we perform the first comprehensive assessment of the influence of the SW external conditions on the SW deflection flow asymmetry in the Martian magnetosheath. More specifically, we analyze the influence of the SW density, velocity and IMF cross-flow component in the observed shocked solar wind deflection asymmetry (Dubinin et al., 2018). To do this, we analyze MAVEN Magnetometer (MAG) and SWIA data between November 2014 and November 2019 (Connerney et al., 2015; Halekas et al., 2015; Jakosky et al., 2015).

2 MAVEN mission and Instruments

The MAVEN spacecraft arrived at Mars in September 2014, and is currently in its extended mission and relay phase. The orbit had a nominal period of about 4.5 hours and an apoapsis altitude of 6220 km (Jakosky et al., 2015), prior to an aerobraking maneuver that lowered apoapsis to $\sim$ 4500 km. MAVEN's orbital precession and apoapsis altitude range allows sampling of both the Martian magnetosheath and the pristine SW. The MAG instrument provides vector magnetic field measurements with two independent fluxgate magnetometers placed on 'boomlets' at the end of the solar array panels. They possess a broad range (up to 65,536 nT per axis), a sampling frequency of 32 Hz, and accuracy of $\sim$0.25 nT (Connerney et al., 2015). In this work we have computed 4s averages based on the full time resolution MAG data. SWIA is an energy and angular ion spectrometer that measures ion flux covering an energy range between 25 eV/q and 25 keV/q (with 48 logarithmically spaced energy steps) with a field of view of $360^\circ \times 90^\circ$ (Halekas et al., 2015). Any moment derived from such flux measurements requires an assumption concerning the ion mass. In this work we have used the onboard computed SW proton density and velocity moments, obtained with a 4s cadence. The computations assume that all ions are protons. This provides a good approximation in the SW and magnetosheath (Halekas, Ruhunusiri, et al., 2017).

MAG data are used to determine the Interplanetary Magnetic Field (IMF) and the SW convective electric field $\mathbf{E}_{SW}$ associated with each analyzed MAVEN orbit. SWIA observations are analyzed to determine $\mathbf{E}_{SW}$, the pristine SW proton density and velocity and to characterize the SW flow asymmetry in the Martian magnetosheath.

3 Selection Criteria

In this work we first identify MAVEN orbits between 12 November 2014 and 30 November 2019 where the spacecraft visited both the upstream SW region and the Martian magnetosheath and where both MAG and SWIA provided measurements. Solar wind external conditions (density, velocity, IMF) associated with each of those orbits are obtained from Halekas, Ruhunusiri, et al. (2017) external averages. The reader is referred to that work for a description. Based on such estimates, we determine the SW velocity components in the Martian magnetosheath in the Mars Solar Electric (MSE) coordinate system. Here, we assume that the SW conditions are approximately constant between the time MAVEN samples the upstream region and measures in the magnetosheath. The MSE coordinate system is defined as follows: the X_{MSE} axis is antiparallel to the upstream average SW velocity, the Y_{MSE} axis points along the cross-flow component of the IMF, and the Z_{MSE} axis points along the SW convective electric field. This is the coordinate system used throughout this work.

If the Martian magnetosphere and the SW are under stationary conditions the Z_{MSE} component of Equation (3) can be rewritten as:

$$V_p^x \frac{dV_p^z}{dx} = -\frac{e\, n_{o^+}}{m_p\, n_{sw}}\, E_{SW}^z \tag{4}$$

which is equal to:

$$\frac{dV_p^z}{dx} = \frac{e\,n_{o^+}}{m_p\,n_{sw}}\,B_y \tag{5}$$

suggesting a dependence between the solar wind flow asymmetry on the $(e\,B_y)/(n_{sw}m_p)$ external factor. Here we use that $n_e \sim n_{sw}$ and that the SW flow is aligned with the X_{MSE} axis upstream from the Martian bow shock (boundary condition).

Figure 1 displays the probability distribution function and the associated quartiles (Q_{25}, Q_{50}, Q_{75}) of the SW proton density, velocity, the Y_{MSE} IMF component and the $(e\,B_y)/(n_{sw}m_p)$ factor upstream from the bow shock, associated with the magnetosheath observations analyzed in the present study.

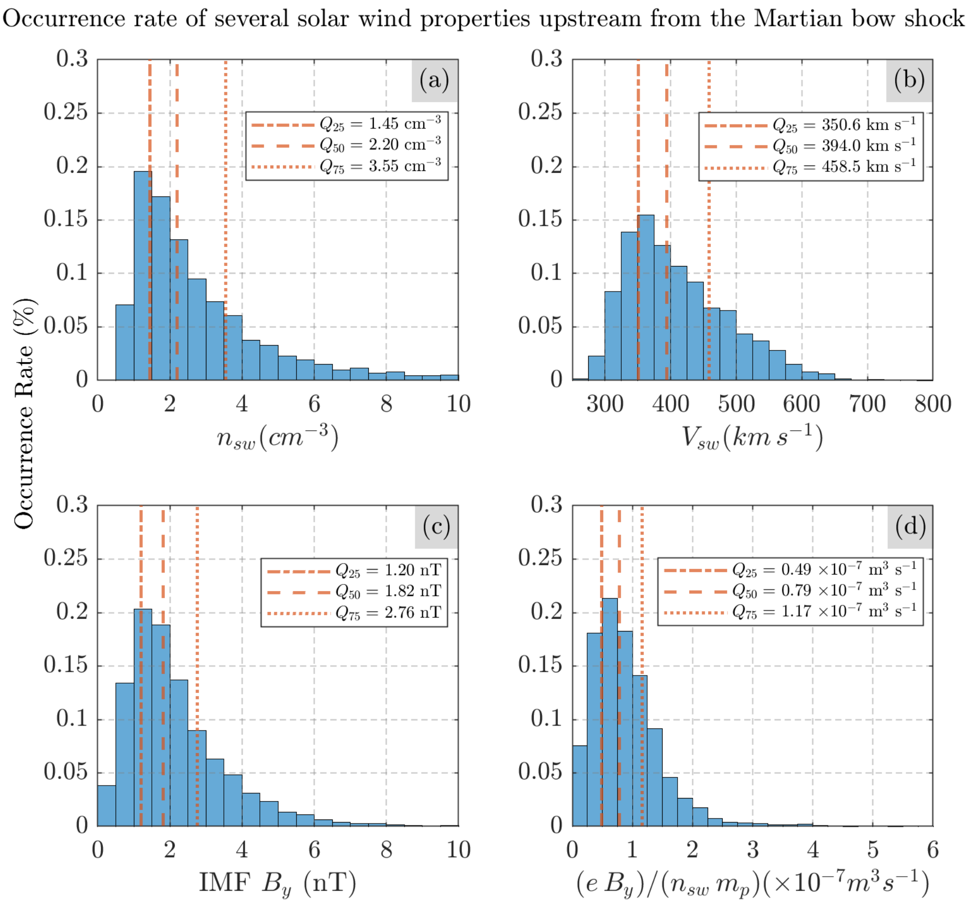

Figure 1. Occurrence rate of the pristine solar wind properties for the orbits analyzed in this study. Panels a)-d) display probability distribution function of the solar wind proton density, velocity, Y_{MSE} IMF component and the $(eB_y)/(n_{sw}m_p)$ factor, respectively. The orange vertical lines correspond to the associated quartiles.

4 Statistical Results and Discussion

4.1 Solar wind flow deflection asymmetry in the Martian magnetosheath

Figure 2a)-d) show the average value of $|V_z|$ (color-coded) as a function of X_{MSE} and Z_{MSE}, where V_z is the Z_{MSE} component of the solar wind velocity. This map is based

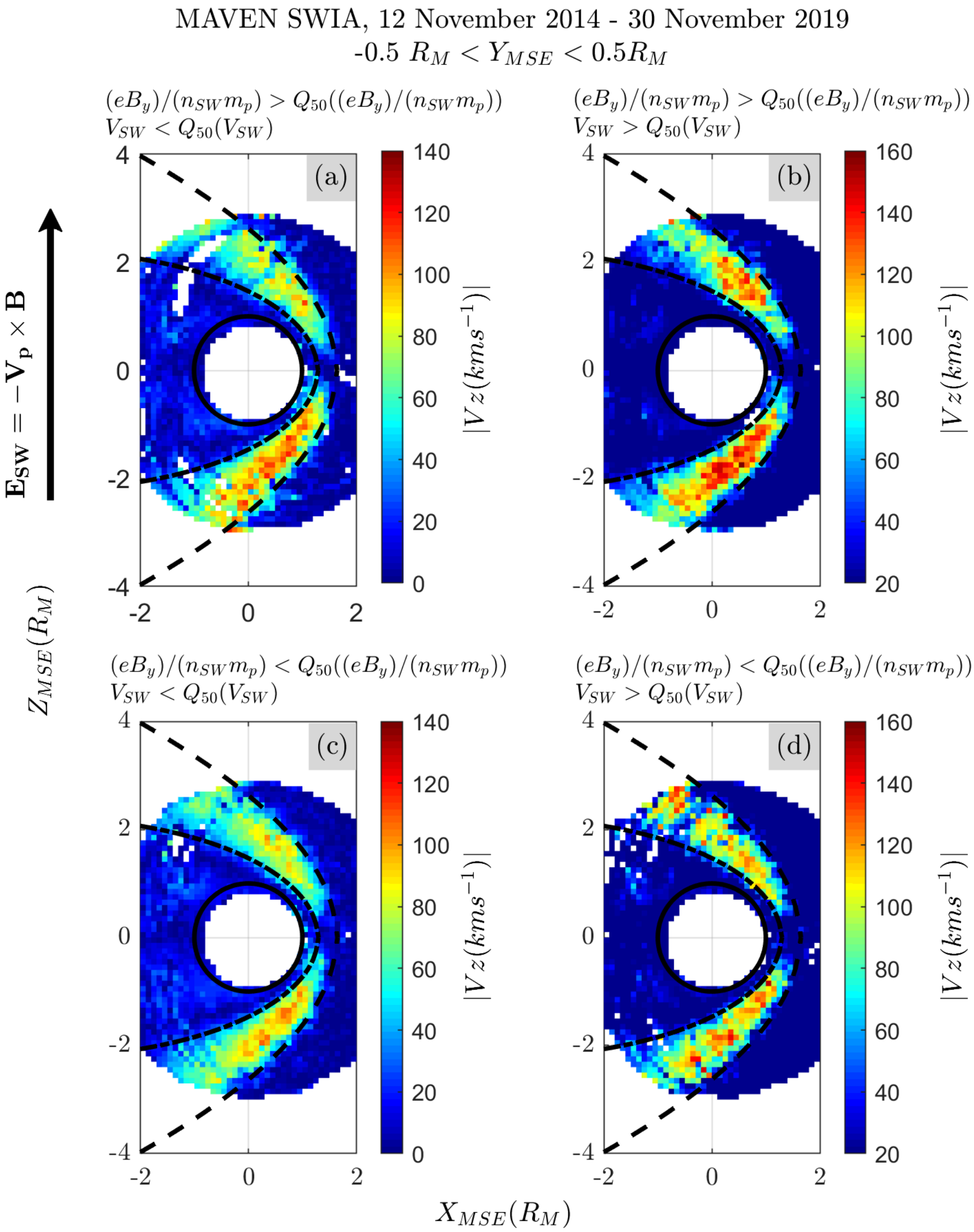

Figure 2. Average value of $|V_z|$ (color-coded) as a function of X_{MSE} and Z_{MSE}, for all selected orbits between 12 November 2014 and 30 November 2019. Upper (lower) panels correspond to measurements associated with relatively strong (weak) forcing $(e\,B_y)/(n_{sw}m_p)$ when compared to the median of the distribution. Left (right) panels correspond to relatively slow (fast) solar wind velocity, when compared to the solar wind velocity median.

on SWIA measurements obtained between $-0.5\,R_M < Y_{MSE} < 0.5\,R_M$.The spatial resolution is $0.1\,R_M \times 0.1\,R_M$. Empty bins in this map correspond to cases with less than 20 measurements, approximately the number of observations obtained by MAVEN when crossing a given bin with a 4s cadence. Mean values of $|V_z|$ presented in each panel correspond to different SW conditions upstream from the Martian bow shock. Figure 2 shows the average $|V_z|$ for four sets of conditions associated with $(e\,B_y)/(n_{sw}m_p)$ and the SW velocity upstream from the bow shock. As shown in Equation (5), the $(e\,B_y)/(n_{sw}m_p)$ quantity is a proxy for the level of solar wind forcing affecting $\frac{dV_p^z}{dx}$. Additionally, changes in $\frac{dV_p^z}{dx}$ are considered significant in relationship with the local SW magnetosheath velocity, that depends, in turn, on the SW velocity upstream from the bow shock.

As can be seen in Figure 2 a),b),c), we find a clear asymmetry in the spatial distribution of $|V_z|$, with larger values in the negative Z_{MSE} hemisphere, opposite to the positive SW convective electric field hemisphere. This result is in agreement with the ones presented in Dubinin et al. (2018). Moreover, these results suggest that the upstream SW conditions have a significant effect on the asymmetry observed in the Martian magnetosheath. For instance, the asymmetry is clearly present in Panel a) and significantly reduced in panel d), confirming our theoretical expectations. Indeed, Panel a) corresponds to the case with relatively strong forcing ($(e\,B_y)/(n_{sw}m_p)$) and slow SW, where the mass-loading effect should be clearly observable. Panel d) constitutes the opposite case, with relatively weak forcing and fast SW. Panel b) and c) are intermediate regimes, where the asymmetry is still clearly noticeable.

4.2 Relation between the solar wind deflection asymmetry and the external conditions

Next, we perform a quantitative analysis to study the relationship between the SW flow asymmetry in the Martian magnetosheath and the SW external conditions. We first focus this part of the analysis at the terminator plane, as $\sim 32\%$ of all analyzed MAVEN's measurements obtained inside the Martian magnetosheath with $|Y_{MSE}| < 0.5\,R_M$ are between $-0.5\,R_M < X_{MSE} < 0.5\,R_M$. Thus, the relatively large fraction of available data in this region allow us to perform a robust statistical analysis. Moreover, as shown in Figure 2, the asymmetry is clearly present around this plane.

As a first step, we compute the mean values and standard deviation of V_z in the Martian magnetosheath at the terminator plane for different SW conditions. Figure 3 shows an example of the mean value of V_z as a function of Y_{MSE} and Z_{MSE}, when the external conditions satisfy that $0.57{\times}10^{-7}$ m^{3}s^{-1} $< eB_y/n_{sw}m_p < 1.23{\times}10^{-7}$ m^{3}s^{-1}, and $Q_{25}(V_{sw}) < V_{sw} < Q_{75}(V_{sw})$. As can be seen, the shocked SW plasma has most of the positive and negative V_z components in the positive and negative electric field hemispheres, respectively.

Based on such mean velocity field maps, we compute the mean value and standard deviation of V_z for two spatial regions inside the Martian magnetosheath. These spatial regions are located in the positive and negative Z_{MSE} hemispheres and are limited by the magnetic pile-up boundary (MPB) and bow shock fits and the $|Y_{MSE}| = \pm 0.5\,R_M$ planes. We implement a conservative approach to ensure the mean values presented hereafter are associated with observations in the magnetosheath by increasing (reducing) the value of the cylindrical radius of the MPB (bow shock) fit at this plane by a factor 1.2, taking into account variability in the boundary locations (Gruesbeck et al., 2018; Vignes et al., 2000). Hereafter, the parameters $\langle Vz^+\rangle$ and $\langle Vz^-\rangle$ are the mean values of V_z associated with such regions, located in the positive and negative SW convective electric field hemispheres, respectively. In the particular case shown in Figure 3, $\langle Vz^+\rangle$ and $\langle Vz^-\rangle$ are equal to 69.1 km s^{-1} and -92.3 km s^{-1}, respectively. The associated standard deviations of each of these means are 0.32 km s^{-1} and 0.31 km s^{-1}, respectively.

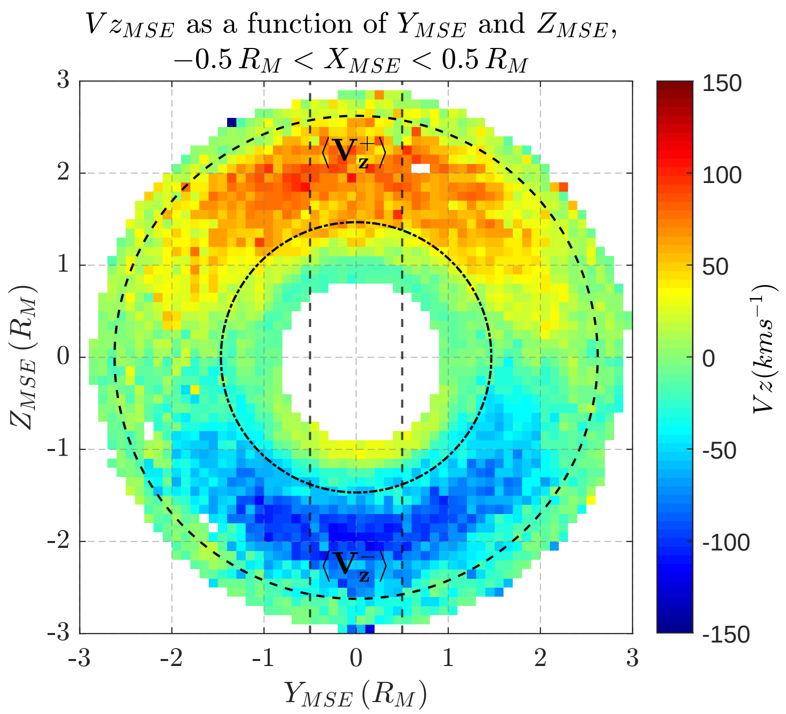

Figure 3. Mean value of the solar wind V_z component between $-0.5\,R_M < X_{MSE} < 0.5\,R_M$, as a function of Y_{MSE} and Z_{MSE}, when 0.57×10^{-7} m^{3}s^{-1} $< eB_y/n_{sw}m_p < 1.23 \times 10^{-7}$ m^{3}s^{-1}, and $Q_{25}(V_{sw}) < V_{sw} < Q_{75}(V_{sw})$. Inner and outer circles correspond to the intersection between the MPB and bow shock fits and the terminator plane, respectively.

We iterate this process for different SW external conditions, computing $\langle Vz^+\rangle$ and $\langle Vz^-\rangle$ when MAVEN's spatial coverage of each of both regions is equal or larger than 80%, and only considering bins with at least 20 measurements when determining these averages.

Figure 4 a), c) and e) display $\langle Vz^+\rangle$ and $\langle Vz^-\rangle$ as a function of the upstream $(e\,B_y)/(n_{sw}m_p)$, B_y and n_{sw}, respectively. To reduce the influence of variability in other external parameters, panel a) considers magnetosheath observations when $Q_{25}(V_{SW}) < V_{SW} < Q_{75}(V_{SW})$, while panel b) and c) consider observations when the pristine solar wind satisfy this condition, in addition to $Q_{25}(n_{SW}) < n_{SW} < Q_{75}(n_{SW})$ and $Q_{25}(B_y) < B_y < Q_{75}(B_y)$, respectively. Panels b), d) and f) display $\langle Vz^+\rangle+\langle Vz^-\rangle$ as a function of the same respective parameters, together with the best liner fit, based on the least square method. Vertical bars in these panels take into account both the standard deviation of each mean ($\langle Vz^+\rangle$ and $\langle Vz^-\rangle$) plus SWIA's instrumental angular and energy resolution (Halekas et al., 2015). The latter factor represents the most important contribution to the uncertainty in $\langle Vz^+\rangle$ and $\langle Vz^-\rangle$ but it might be overestimated, depending on the width of the local velocity distribution function. In addition, these bars also take into account that the SWIA on-board moment calculation assumes that the magnetosheath plasma is totally composed of protons, thus overestimating the local flow speed by a factor $\sqrt{m_{o+}/m_p}$ for the portion of the flow composed of oxygen ions (Halekas, Ruhunusiri, et al., 2017). By considering a magnetosheath plasma made of $n_e = 10$ cm^{-3} and $n_{o+} = 0.1\,$cm^{-3}

(Dubinin et al., 2018; Romanelli et al., 2018) we estimate that the velocity components might be overestimated by a factor ~ 1.07 due to this assumption.

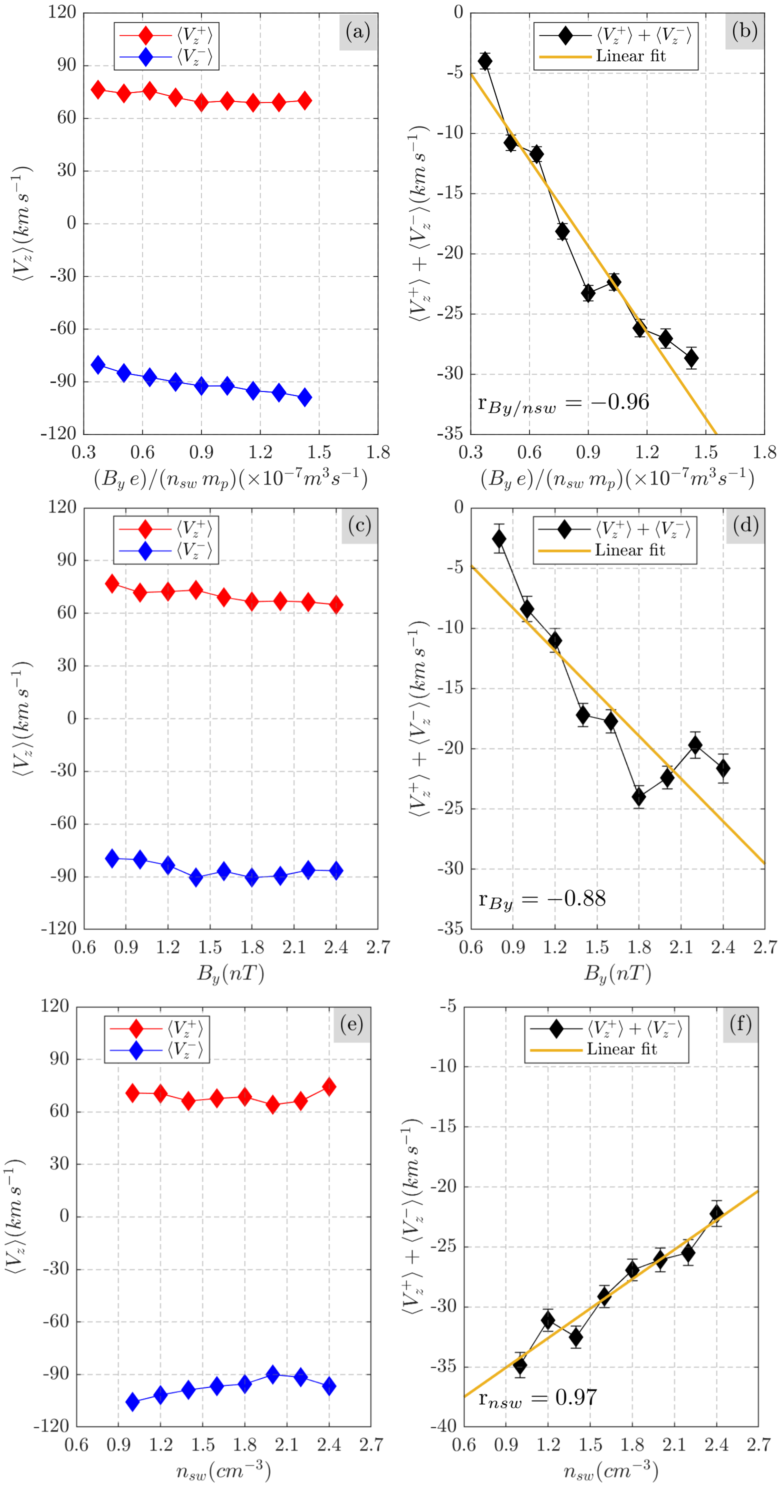

Figure 4. Solar wind flow asymmetry ($\langle Vz^+ \rangle$, $\langle Vz^- \rangle$ and $\langle Vz^+ \rangle + \langle Vz^- \rangle$) in the magnetosheath as a function of the upstream $(e\,B_y)/(n_{sw} m_p)$, B_y and n_{sw}.

As can be seen in Figure 4, left panels, $|\langle Vz^+ \rangle|$ is systematically smaller than $|\langle Vz^- \rangle|$, for all the external conditions explored in this study, between 12 November 2014 and 30 November 2019. This asymmetry is consistent with results shown in Figure 2 in Dubinin et al. (2018), associated with averaged conditions between November 2014 and May 2016. Moreover, the right panels show that $\langle Vz^+\rangle + \langle Vz^-\rangle$ displays an approximate linear dependence with the three external parameters. In particular, the linear fit shown Figure 4b) is characterized by a slope ($m_{By/nsw}$) equal to (-23.9 ± 0.7) $\times10^{10}$ m^{-2}, a y-intercept ($b_{By/nsw}$) equal to (2.1 ± 0.7) $\times$ 10^3 m s^{-1}, a linear correlation coefficient $r_{By/nsw}$ = -0.96 and a p-value ($p_{By/nsw}$) equal to 2.9×10^{-5}. The 95% confidence $r_{By/nsw}$ interval is [-0.99 - (-0.83)]. These results suggest the presence of a linear correlation between the SW flow asymmetry in the magnetosheath at the terminator plane and the $(e\,B_y)\,/(n_{sw}m_p)$ value upstream from the bow shock. Moreover, we also observe a linear relationship between $\langle Vz^+\rangle + \langle Vz^-\rangle$ and B_y and n_{sw}, independently, as shown in Figure 4d) and f). The associated slopes are (-11.8 ± 0.7) $\times10^{12}$ m s^{-1}T^{-1} and (8.2 ± 0.8) $\times10^{-3}$ m^4 s^{-1}, while the associated y-intercepts are $(2.3 \pm 1.2) \times 10^3$ m s^{-1} and $(-42.4 \pm 1.4) \times 10^3$ m s^{-1}, respectively. The associated linear correlation coefficients (r_{By}, r_{nsw}) are -0.88 and 0.97, and the corresponding 95% confidence r-interval are [-0.98 - (-0.53)] and [0.84 - 0.99], respectively. The associated p-values are 1.6×10^{-3} and 6.3×10^{-5}. These results also suggest that there is a linear relationship between the magnetosheath SW flow asymmetry and the SW proton density and B_y IMF component, upstream from the bow shock. The presence of a departure from a linear trend in panel d), for $B_y \gtrsim 1.8$ nT, may indicate that when the IMF intensity increases, the Larmor gyroradii of the planetary heavy ions is reduced, thus the characteristic size of the O^+ plume is reduced, and therefore these conditions may reduce the deflection of SW protons in the Martian magnetosheath as well.

As previously mentioned, an additional factor can introduce uncertainties in the reported values of V_z. Indeed, the computation of the SW velocity MSE components assumes that the SW velocity and IMF did not vary significantly over one MAVEN orbit. However, by performing a statistical analysis using 5 years of data, we are able to apply strict selection criteria (selected orbits, coverage in the magnetosheath, number of measurements per bin) seeking to reduce effects of potential outliers, when such transformation into the MSE coordinate system is performed. Indeed, these outliers could be the result of temporal variability in the external conditions.

Finally, we analyze the variability of the observed flow asymmetry with the upstream $(e\,B_y)\,/(n_{sw}m_p)$, by computing analogous linear fits using SWIA data inside the magnetosheath with $|Y_{MSE}| < 0.5\,R_M$ for $X_{MSE} = [(-1) - 0]\,\mathrm{R}_M$ and $X_{MSE} = [0 - 1]\,R_M$. We focus this part of the analysis only on the dependence with $(e\,B_y)\,/(n_{sw}m_p)$, as the statistics to study the dependence with the other two parameters (independently) at these planes is relatively poor. The results are presented in Table 1. As can be seen, a linear dependence is also observed in these regions with linear correlation coefficients ~ -0.9 and p-values $\sim 1 \times 10^{-4}$, suggesting the correlations are significant. Finally, we report that we did not find any significant correlation between the shocked SW flow asymmetry and the upstream SW velocity, in agreement with expectations from Equation 5 (not shown).

Linear fit parameters	$X_{MSE} = -0.50\,R_M$	$X_{MSE} = 0\,R_M$	$X_{MSE} = 0.5\,R_M$
$m_{By/nsw}$	(-16.4 ± 0.6)$\times10^{10}$ m^{-2}	(-23.9 ± 0.7)$\times10^{10}$ m^{-2}	$(-15.6\pm1.0)\times10^{10}$ m^{-2}
$b_{By/nsw}$	(5.7 ± 0.6)$\times10^3$ m s^{-1}	$(2.1 \pm 0.7)\times10^3$ m s^{-1}	(8.8 ± 0.9) $\times10^3$ m s^{-1}
$r_{By/nsw}$	-0.93 [-0.98 - (-0.72)]	-0.96 [-0.99 - (-0.83)]	-0.93 [-0.99 - (-0.71)]
$p_{By/nsw}$	1.0×10^{-4}	2.9×10^{-5}	2.2×10^{-4}

Table 1. Parameters associated with the linear fit between the magnetosheath $\langle Vz^+\rangle + \langle Vz^-\rangle$ and upstream $(e\,B_y)\,/(n_{sw}m_p)$ for different X_{MSE} planes.

5 Conclusions

In this work we have characterized the SW deflection asymmetry in the Martian magnetosheath, making use of ~ 5 years of MAVEN MAG and SWIA observations. In agreement with Dubinin et al. (2018), our results suggest that this asymmetry (in the $\mathbf{V}_{SW}-\mathbf{E}_{SW}$ plane) can be understood in terms of a bi-fluid description. Moreover, it constitutes a signature associated with the conservation of the total linear momentum of the SW massloaded with O^+ ions, where the latter are preferentially accelerated along the SW convective electric field.

In addition, we have also quantified, for the first time, the effects that several SW external conditions have on such asymmetry. In particular, we find a linear relationship between a measure of the plasma flow asymmetry inside the magnetosheath and around the terminator plane ($\langle Vz^+\rangle+\langle Vz^-\rangle$) and the IMF cross-flow component, the SW proton density, and the $(e\,B_y)\,/(n_{sw}m_p)$ external factor. In particular, we observe that the asymmetry increases with the IMF cross-flow component, and is reduced for denser SW conditions. These results are in agreement with theoretical expectations derived from the bi-fluid model. Finally, a similar dependence between the magnetosheath plasma flow asymmetry and the ratio between the IMF cross-flow component and the SW proton density is observed around $X_{MSO} = -0.50\,R_M$ and $X_{MSO} = 0.5\,R_M$.

A future study will focus on the analysis of the spatial variability of this asymmetry, and its dependence on other internal/external parameters. This work will be based on numerical simulations and oxygen ion densities derived from MAVEN STATIC instrument.

Acknowledgments

N.R. is an Assistant Research Scientist at NASA Goddard Space Flight Center, hired by MAVEN Project Scientist Support, and administrated by Center for Research and Exploration in Space Sciences & Technology II and University of Maryland Baltimore County (UMBC). MAVEN data used in this study are publicly available through the Planetary Data System (https://pds-ppi.igpp.ucla.edu/).

References

Acuña, M. H., Connerney, J. E. P., Wasilewski, P., Lin, R. P., Anderson, K. A., Carlson, C. W., ... Ness, N. F. (1998). Magnetic Field and Plasma Observations at Mars: Initial Results of the Mars Global Surveyor Mission. *Science*, *279*(5357), 1676–1680. doi: 10.1126/science.279.5357.1676

Andrés, N., Romanelli, N., Hadid, L. Z., Sahraoui, F., DiBraccio, G., & Halekas, J. (2020). Solar Wind Turbulence Around Mars: Relation between the Energy Cascade Rate and the Proton Cyclotron Waves Activity. *The Astrophysical Journal*, *902*(2), 134. doi: 10.3847/1538-4357/abb5a7

Barabash, S., Dubinin, E., Pissarenko, N., Lundin, R., & Russell, C. T. (1991). Picked-up protons near Mars: Phobos observations. *Geophysical Research Letters*, *18*(10), 1805-1808. doi: 10.1029/91GL02082

Behar, E., Lindkvist, J., Nilsson, H., Holmström, M., Stenberg-Wieser, G., Ramstad, R., & Götz, C. (2016). Mass-loading of the solar wind at 67P/Churyumov-Gerasimenko - Observations and modelling. *A&A*, *596*, A42. Retrieved from `https://doi.org/10.1051/0004-6361/201628797` doi: 10.1051/0004-6361/201628797

Behar, E., Nilsson, H., Alho, M., Goetz, C., & Tsurutani, B. (2017). The birth and growth of a solar wind cavity around a comet – Rosetta observations. *Monthly Notices of the Royal Astronomical Society*, *469*(Suppl 2), S396-S403. Retrieved from `https://doi.org/10.1093/mnras/stx1871` doi:

10.1093/mnras/stx1871

Bertucci, C., Romanelli, N., Chaufray, J.-Y., Gomez, D., Mazelle, C., Delva, M., ... Brain, D. A. (2013). Temporal variability of waves at the proton cyclotron frequency upstream from Mars: Implications for Mars distant hydrogen exosphere. *Geophysical Research Letters*, *40*(15), 3809–3813. doi: 10.1002/grl.50709

Brain, D. A., Bagenal, F., Acuña, M. H., Connerney, J. E. P., Crider, D. H., Mazelle, C., ... Ness, N. F. (2002). Observations of low-frequency electromagnetic plasma waves upstream from the Martian shock. *Journal of Geophysical Research: Space Physics*, *107*(A6). doi: 10.1029/2000JA000416

Broiles, T., Burch, J. L., Clark, G., Koenders, C., Behar, E., Goldstein, R., ... Samara, M. (2015). Rosetta observations of solar wind interaction with the comet 67P/Churyumov-Gerasimenko. *A&A*, *583*, A21. Retrieved from `https://doi.org/10.1051/0004-6361/201526046` doi: 10.1051/0004-6361/201526046

Chaffin, M. S., Chaufray, J.-Y., Deighan, J., Schneider, N. M., McClintock, W. E., Stewart, A. I. F., ... Jakosky, B. M. (2015). Three-dimensional structure in the Mars H corona revealed by IUVS on MAVEN. *Geophysical Research Letters*, *42*(21), 9001–9008. doi: 10.1002/2015GL065287

Chaffin, M. S., Chaufray, J.-Y., Stewart, I., Montmessin, F., Schneider, N. M., & Bertaux, J.-L. (2014). Unexpected variability of Martian hydrogen escape. *Geophysical Research Letters*, *41*(2), 314–320. doi: 10.1002/2013GL058578

Chaufray, J.-Y., Bertaux, J.-L., Leblanc, F., & Quémerais, E. (2008). Observation of the hydrogen corona with SPICAM on Mars Express. *Icarus*, *195*(2), 598–613. doi: 10.1016/j.icarus.2008.01.009

Clarke, J. T., Mayyasi, M., Bhattacharyya, D., Schneider, N. M., Mcclintock, W. E., Deighan, J. I., ... Jakosky, B. M. (2017). Variability of D and H in the Martian upper atmosphere observed with the MAVEN IUVS echelle channel. *Journal of Geophysical Research: Space Physics*, *122*(2), 2336–2344. doi: 10.1002/2016JA023479

Connerney, J. E. P., Espley, J., Lawton, P., Murphy, S., Odom, J., Oliversen, R., & Sheppard, D. (2015). The MAVEN magnetic field investigation. *Space Science Reviews*, *195*(1-4), 257–291. doi: 10.1007/s11214-015-0169-4

Curry, S. M., Luhmann, J. G., Ma, Y. J., Dong, C. F., Brain, D., Leblanc, F., ... Jakosky, B. (2015). Response of Mars O+ pickup ions to the 8 March 2015 ICME: Inferences from MAVEN data-based models. *Geophysical Research Letters*, *42*(21), 9095-9102. doi: 10.1002/2015GL065304

Deighan, J., Chaffin, M. S., Chaufray, J.-Y., Stewart, A. I. F., Schneider, N. M., Jain, S. K., ... Jakosky, B. M. (2015). MAVEN IUVS observation of the hot oxygen corona at Mars. *Geophysical Research Letters*, *42*(21), 9009-9014. doi: 10.1002/2015GL065487

Dong, Y., Fang, X., Brain, D. A., McFadden, J. P., Halekas, J. S., Connerney, J. E., ... Jakosky, B. M. (2015). Strong plume fluxes at Mars observed by MAVEN: An important planetary ion escape channel. *Geophysical Research Letters*, *42*(21), 8942-8950. doi: 10.1002/2015GL065346

Dubinin, E., Fraenz, M., Pätzold, M., Halekas, J. S., Mcfadden, J., Connerney, J. E. P., ... Zelenyi, L. (2018). Solar Wind Deflection by Mass Loading in the Martian Magnetosheath Based on MAVEN Observations. *Geophysical Research Letters*, *45*(6), 2574-2579. doi: 10.1002/2017GL076813

Dubinin, E., Fraenz, M., Woch, J., Barabash, S., Lundin, R., & Yamauchi, M. (2006). Hydrogen exosphere at Mars: Pickup protons and their acceleration at the bow shock. *Geophysical Research Letters*, *33*(22). doi: 10.1029/2006GL027799

Feldman, P. D., Steffl, A. J., Parker, J. W., A'Hearn, M. F., Bertaux, J.-L., Alan Stern, S., ... Feaga, L. M. (2011). Rosetta-Alice observations of exospheric hydrogen and oxygen on Mars. *Icarus*, *214* (2), 394 - 399. doi: https://doi.org/10.1016/j.icarus.2011.06.013

Glassmeier, K.-H. (2017). Interaction of the solar wind with comets: a Rosetta perspective. *Philosophical Transactions of the Royal Society A: Mathematical, Physical and Engineering Sciences*, *375* (2097), 20160256. doi: 10.1098/rsta.2016.0256

Gruesbeck, J. R., Espley, J. R., Connerney, J. E. P., DiBraccio, G. A., Soobiah, Y. I., Brain, D., ... Mitchell, D. L. (2018). The three-dimensional bow shock of Mars as observed by MAVEN. *Journal of Geophysical Research: Space Physics*, *123* (6), 4542–4555. doi: 10.1029/2018JA025366

Halekas, J. S. (2017). Seasonal variability of the hydrogen exosphere of Mars. *Journal of Geophysical Research: Planets*, *122* (5), 901–911. doi: 10.1002/2017JE005306

Halekas, J. S., Brain, D. A., Luhmann, J. G., DiBraccio, G. A., Ruhunusiri, S., Harada, Y., ... Jakosky, B. M. (2017). Flows, Fields, and Forces in the Mars-Solar Wind Interaction. *Journal of Geophysical Research: Space Physics*, *122* (11), 11,320-11,341. doi: 10.1002/2017JA024772

Halekas, J. S., Ruhunusiri, S., Harada, Y., Collinson, G., Mitchell, D. L., Mazelle, C., ... Jakosky, B. M. (2017). Structure, dynamics, and seasonal variability of the Mars-solar wind interaction: MAVEN Solar Wind Ion Analyzer in-flight performance and science results. *Journal of Geophysical Research: Space Physics*, *122* (1), 547-578. doi: 10.1002/2016JA023167

Halekas, J. S., Ruhunusiri, S., Vaisberg, O. L., Harada, Y., Espley, J. R., Mitchell, D. L., ... Brain, D. A. (2020). Properties of Plasma Waves Observed Upstream From Mars. *Journal of Geophysical Research: Space Physics*, *125* (9), e2020JA028221. doi: 10.1029/2020JA028221

Halekas, J. S., Taylor, E. R., Dalton, G., Johnson, G., Curtis, D. W., McFadden, J. P., ... Jakosky, B. M. (2015). The solar wind ion analyzer for MAVEN. *Space Science Reviews*, *195* (1-4), 125–151. doi: 10.1007/s11214-013-0029-z

Jakosky, B. M., Lin, R. P., Grebowsky, J. M., Luhmann, J. G., Mitchell, D. F., Beutelschies, G., ... others (2015). The Mars atmosphere and volatile evolution (MAVEN) mission. *Space Science Reviews*, *195* (1-4), 3–48. doi: 10.1007/s11214-015-0139-x

Liu, D., Yao, Z., Wei, Y., Rong, Z., Shan, L., Arnaud, S., ... Wan, W. (2020). Upstream proton cyclotron waves: occurrence and amplitude dependence on IMF cone angle at Mars—from MAVEN observations. *Earth and Planetary Physics*, *4* (1), 51–61. doi: 10.26464/epp2020002

Mazelle, C., Winterhalter, D., Sauer, K., Trotignon, J. G., Acuna, M. H., Baumgärtel, K., ... Slavin, J. (2004). Bow shock and upstream phenomena at Mars. *Space Science Reviews*, *111*, 115–181. doi: 10.1023/B:SPAC.0000032717.98679.d0

McFadden, J. P., Kortmann, O., Curtis, D., Dalton, G., Johnson, G., Abiad, R., ... Jakosky, B. (2015, December). MAVEN SupraThermal and Thermal Ion Compostion (STATIC) Instrument. , *195* (1-4), 199-256. doi: 10.1007/s11214-015-0175-6

Nilsson, H., Stenberg Wieser, G., Behar, E., Wedlund, C. S., Gunell, H., Yamauchi, M., ... Rubin, M. (2015). Birth of a comet magnetosphere: A spring of water ions. *Science*, *347* (6220). doi: 10.1126/science.aaa0571

Nilsson, H., Wieser, G. S., Behar, E., Gunell, H., Wieser, M., Galand, M., ... Vigren, E. (2017). Evolution of the ion environment of comet 67P during the Rosetta mission as seen by RPC-ICA. *Monthly Notices of the Royal Astronomical Society*, *469* (Suppl 2), S252-S261. Retrieved from `https://doi.org/10.1093/mnras/stx1491` doi: 10.1093/mnras/stx1491

Rahmati, A., Larson, D. E., Cravens, T. E., Lillis, R. J., Dunn, P. A., Halekas, J. S., ... Jakosky, B. M. (2015). MAVEN insights into oxygen pickup ions at Mars.

Geophysical Research Letters, *42*(21), 8870-8876. doi: 10.1002/2015GL065262

Rahmati, A., Larson, D. E., Cravens, T. E., Lillis, R. J., Halekas, J. S., McFadden, J. P., … Jakosky, B. M. (2017). MAVEN measured oxygen and hydrogen pickup ions: Probing the Martian exosphere and neutral escape. *Journal of Geophysical Research: Space Physics*, *122*(3), 3689–3706. doi: 10.1002/2016JA023371

Romanelli, N., Bertucci, C., Gomez, D., Mazelle, C., & Delva, M. (2013). Proton Cyclotron Waves Upstream from Mars: Observations from Mars Global Surveyor. *Planetary and Space Science*, *76*, 1–9. doi: 10.1002/2015GL064968

Romanelli, N., Mazelle, C., Chaufray, J.-Y., Meziane, K., Shan, L., Ruhunusiri, S., … Jakosky, B. M. (2016). Proton cyclotron waves occurrence rate upstream from Mars observed by MAVEN: Associated variability of the Martian upper atmosphere. *Journal of Geophysical Research: Space Physics*, *121*(11), 11–113. doi: 10.1002/2016JA023270

Romanelli, N., Modolo, R., Leblanc, F., Chaufray, J.-Y., Martinez, A., Ma, Y., … Holmström, M. (2018). Responses of the Martian Magnetosphere to an Interplanetary Coronal Mass Ejection: MAVEN Observations and LatHyS Results. *Geophysical Research Letters*, *45*(16), 7891-7900. doi: 10.1029/2018GL077714

Ruhunusiri, S., Halekas, J. S., Connerney, J. E. P., Espley, J. R., McFadden, J. P., Larson, D. E., … Jakosky, B. M. (2015). Low-frequency waves in the Martian magnetosphere and their response to upstream solar wind driving conditions. *Geophysical Research Letters*, *42*(21), 8917–8924. doi: 10.1002/2015GL064968

Ruhunusiri, S., Halekas, J. S., Connerney, J. E. P., Espley, J. R., McFadden, J. P., Mazelle, C., … others (2016). MAVEN observation of an obliquely propagating low-frequency wave upstream of Mars. *Journal of Geophysical Research: Space Physics*, *121*(3), 2374–2389. doi: 10.1002/2015JA022306

Russell, C. T., Luhmann, J. G., Schwingenschuh, K., Riedler, W., & Yeroshenko, Y. (1990). Upstream waves at Mars: Phobos observations. *Geophysical Research Letters*, *17*(6), 897–900. doi: 10.1029/GL017i006p00897

Sauer, K., Bogdanov, A., & Baumgärtel, K. (1994). Evidence of an ion composition boundary (protonopause) in bi-ion fluid simulations of solar wind mass loading. *Geophysical Research Letters*, *21*(20), 2255-2258. doi: 10.1029/94GL01691

Vignes, D., Mazelle, C., Rme, H., Acuña, M. H., Connerney, J. E. P., Lin, R. P., … Ness, N. F. (2000). The solar wind interaction with Mars: Locations and shapes of the bow shock and the magnetic pile-up boundary from the observations of the MAG/ER Experiment onboard Mars Global Surveyor. *Geophysical Research Letters*, *27*(1), 49-52. doi: 10.1029/1999GL010703

Yamauchi, M., Hara, T., Lundin, R., Dubinin, E., Fedorov, A., Sauvaud, J.-A., … others (2015). Seasonal variation of Martian pick-up ions: Evidence of breathing exosphere. *Planetary and Space Science*, *119*, 54–61. doi: 10.1016/j.pss.2015.09.013